

ULTRAFINE PARTICLES IN THE LOWER TROPOSPHERE

Major Sources, Invisible Plumes, and Meteorological Transport Processes

WOLFGANG JUNKERMANN AND JORG M. HACKER

A decade of airborne regional-scale measurements of aerosol size distributions and meteorological parameters allows apportionment of major sources and budget estimates for ultrafine particles.

Ultrafine particles (UFPs) in the atmosphere (diameter <100 nm) have a major impact on the environment through a wide variety of processes. They provide reaction surfaces for heterogeneous chemical processes in the atmosphere or can act as cloud condensation nuclei (CCN). While fine particles (>100 nm) interact directly with shortwave radiation, UFPs do not. Yet UFPs affect short- and

longwave radiation indirectly, by way of their interactions with cloud microphysics. Once UFPs reach sizes larger than 40 nm, they effectively contribute to CCN (Twomey 1977; Andreae 2009; Ma et al. 2016), which then can enhance the number of cloud droplets at the expense of cloud droplet size (Rosenfeld et al. 2008; Leaitch et al. 2010; Junkermann et al. 2009). Subsequent changes in cloud brightness and lifetime are well established (Twomey 1974; Albrecht 1989). These effects have even been proposed as a potentially exploitable physical process for geoengineering (Latham et al. 2008). Yet the concurrent reduction of cloud droplet size modes may have unwanted side effects, such as changes of the distribution and intensity of rainfall on a larger scale (Rosenfeld 2000; Teller and Levin 2006; Teller et al. 2012; Junkermann et al. 2011b; Fan et al. 2018) that, in turn, affects the hydrological cycle (Bister and Kulmala 2011; Riuttanen et al. 2016).

Techniques for the detection of UFPs, condensation particle counters (CPC), were developed more than a hundred years ago by Coulier (1875) and Aitken (1889). Since then, UFPs have been measured in polluted urban and industrial environments, as well as in remote locations. For a historic review, see Mohnen and Hidy (2010). For airborne applications, Bigg and Turvey (1978) and Ayers et al. (1979)

AFFILIATIONS: JUNKERMANN—Karlsruhe Institute of Technology, Institute of Meteorology and Climate Research, Garmisch-Partenkirchen, Germany, and Flinders University, Adelaide, South Australia, Australia; HACKER—Airborne Research Australia, Parafield Airport, and Flinders University, Adelaide, South Australia
CORRESPONDING AUTHOR: Wolfgang Junkermann, wolfgang.junkermann@kit.edu

The abstract for this article can be found in this issue, following the table of contents.

DOI:10.1175/BAMS-D-18-0075.1

In final form 21 August 2018

©2018 American Meteorological Society

For information regarding reuse of this content and general copyright information, consult the [AMS Copyright Policy](#).



This article is licensed under a [Creative Commons Attribution 4.0 license](#).

used continuously recording counters (Pollak and Metnieks 1959) with comparatively low (~1 min) time resolution, but size detection limits were already similar to today's sensors, reaching well into the <10-nm range (Hogan et al. 1981).

The relative scales of number concentrations reported over more than a century have not changed much (Aitken 1894; Landsberg 1938; Went 1964, 1966). Burning of fossil fuel, vehicular traffic, and industry emissions always dominated the UFP number concentrations [see Aitken (1894) and Landsberg (1938) for early reviews; Bigg and Turvey (1978) for characteristic concentrations of remote maritime and continental areas and city plumes in Australia in the early 1970s]. In the first decades of the twentieth century, number concentrations in cities were reported to be very high (Landsberg 1938) but later decreased as a result of emission control measures, from values of $>10^6$ to about 10^5 cm^{-3} in current urban environments (Bae et al. 2010). Traffic is now considered to be the main urban source for UFPs (Paasonen et al. 2016; Rönkkö et al. 2017).

Although UFP concentrations are normally far lower in rural regions than in urban or industrial areas, number concentration magnitudes comparable to urban roadside levels have been detected even in very remote areas over the last three decades. Typically these are associated with short-duration particle burst events (Kulmala et al. 2004). During such events, which are classified in the recent literature as new particle formation (NPF), number concentrations increase rapidly by an order of magnitude within less than an hour during mid- to late morning hours. Initially, tiny particles appear in the smaller size bins of particle spectrometers [scanning mobility particle sizer (SMPS)] (~5–20 nm). Subsequent shifts by a few nanometers per hour indicate particle growth, while number concentrations are decreasing (Kulmala and Kerminen 2008; Kulmala et al. 2013; Tröstl et al. 2016). This process, resulting in “banana”-shaped patterns in diurnal size distribution plots, is typically observed under sunny meteorological conditions (Baranizadeh et al. 2014) and more often in spring than in summer (Dal Maso et al. 2005). Nighttime events were occasionally reported with growth less significant than during the day or not occurring at all (Suni et al. 2008). Such events have not been reported in the literature before 1990 but are now observed even at remote locations, such as Arctic and Antarctic regions (Kontkanen et al. 2017; Heintzenberg et al. 2017).

Kiang et al. (1973), Kulmala et al. (2013), and Petäjä et al. (2016) suggested that atmospheric gas-to-particle conversion (GPC), the formation of H_2SO_4

from photochemical sulfur dioxide oxidation via hydroxide (OH) radicals, would be a key process for the production of initial aerosol clusters. These would then react with ammonia and/or amines via ternary nucleation. Subsequent particle growth could then be related to organic compounds, such as extremely low-volatility organic compounds (ELVOC), emitted from the biosphere (Ehn et al. 2014; Dall'Osto et al. 2018). A contribution of ELVOC is in agreement with the observation of UFP growth over mild to moderately polluted mid-European forested areas (Kulmala et al. 2004; Held et al. 2004). However, it is interesting to note that the frequency of observations does not follow the annual patterns of biogenic emissions. It also remains unclear where and what the source of H_2SO_4 would be.

When compared to anthropogenic emissions from power stations, biogenic emissions typically have far lower spatial and temporal variability of the source strength and usually exhibit a considerably more homogeneous distribution. Also, characteristic UFP burst events are not common in “clean” forested areas over Australia and the Amazon that are clearly dominated by biogenic emissions (Junkermann et al. 2009; Junkermann and Hacker 2015; Fan et al. 2018; Andreae et al. 2018). Other recent observations of pronounced horizontal (on scales of less than 50 km) and vertical UFP variability, UFP layers just at the top of the PBL, and size distributions with a clear nucleation mode at about 5–10 nm but lower number concentrations below 5 nm cannot be explained by biogenic emissions (Ma and Birmili 2015; Crippa et al. 2012; Crumeyrolle et al. 2010; Schobesberger et al. 2013; Väänänen et al. 2016; Heintzenberg et al. 2007; Kulmala et al. 2013). Anthropogenic UFPs from elevated stack emissions transported by horizontal advection and vertical convection processes do not only fit these UFP scenarios better than NPF but can also offer an explanation for their increased occurrence within the last decades.

This paper attempts to corroborate this notion based on airborne measurements of UFPs using highly flexible, well-instrumented aircraft together with meteorological observations and transport model analysis.

Connecting the short-duration UFP events with meteorological convective vertical transport and horizontal advection requires a reliable method of source apportionment and characterization of relevant transport mechanisms. Attempts at such source apportionment of UFP production in the lower troposphere have been made ever since particle instrumentation became available at the end

of the nineteenth century (Aitken 1894). Aircraft-based measurements, coordinated with ground observations, were used recently in several projects: Quantification of Aerosol Nucleation in the European Boundary Layer (QUEST; Laaksonen et al. 2005, 2008), European Integrated Project on Aerosol Cloud Climate and Air Quality Interactions (EUCAARI; Kulmala et al. 2011; Schobesberger et al. 2013), and Biogenic Aerosols—Effects on Clouds and Climate (BAECC; Väänänen et al. 2016; Petäjä et al. 2016). However, even after these detailed international field studies, the sources and budgets of anthropogenic ultrafine aerosols remain highly uncertain (Dall’Osto et al. 2018).

In our studies, based on detailed airborne observations using small and slow-flying instrumented aircraft, we were able to characterize major UFP sources, their quantitative contribution to the total budget of UFPs, and how local nucleation mode particle appearance may be linked to elevated particle sources via meteorological processes. We hypothesize that particles attributable to flue-gas-cleaning efforts, established since the late 1980s, have resulted in a substantial increase in primary nucleation size mode particles and are now a major contribution to the anthropogenic budget of UFPs. This change in emissions may also be the relevant process to explain the worldwide increase of nucleation mode particles.

The present study is organized in two sections. First, we discuss the meteorology behind the three-dimensional transport within the time scales of UFP lifetime. Second, we describe selected experimental data confirming the horizontal and vertical aerosol patterns.

METEOROLOGY RELATED TO DIURNAL THREE-DIMENSIONAL UFP DISTRIBUTIONS.

Meteorological processes play a major role in the interpretation of the observed temporal and spatial patterns of UFPs. The typical emissions from elevated smoke stacks that form plumes with high UFP number concentrations offer opportunities for detailed case studies on the impact of meteorological transport phenomena on the three-dimensional distribution of UFPs. Both the lifetime of UFPs and their growth processes take place at similar time scales as regional-scale horizontal transport (i.e., between one and a few days). In contrast thereto, convective vertical transport occurs at time scales of less than 1 h and is rapid compared to aerosol aging processes (Georgii 1956; Stull 1988; Kulmala et al. 2013). Physical properties of the aerosol are thus preserved during vertical transport by thermal convection (Bigg et al. 1978) but

may change during horizontal transport. Horizontal transport typically dominates during stable stratification of the lower atmosphere, at night or under daytime overcast conditions.

The emission of UFPs into the lower atmosphere from flue gas stacks (Junkermann et al. 2011a) typically takes place at heights of 200–400 m AGL, depending on stack height and excess flue gas temperatures. In daytime conditions, this release height puts the emissions well into the mid-PBL, with convective turbulence distributing the UFPs in both directions, down to the ground and up toward the cloud base. Elevated emission altitude with rapid vertical mixing (Buzorius et al. 2001; Wehner et al. 2010) typically leads to plumes reaching the ground at most by about ~2–5 km downwind of the stack, with UFP concentrations subsequently diminished by dispersion and deposition losses. At nighttime, while wind speed usually decreases markedly in the surface layer, values of 5–10 m s⁻¹ are still typical above the nocturnal inversion and can reach considerably higher values over large flat landscapes. Thus, during the night hours a high concentration layer of particles can form within the less turbulent residual layer (RL), containing remaining PBL air and fresh emissions injected above the nocturnal inversion layer of ~100–150 m. Such conditions may extend over hundreds of kilometers, with little vertical mixing (Ayers et al. 1979; Junkermann et al. 2011b). Under clear or only low-cloud-cover conditions such nocturnal layering is broken up the next morning by thermal convection, and UFPs from far-distant elevated sources can reach the ground by fumigation. The highest concentrations close to the ground are thus often found about 30 min after thermal convection reaches the altitude of the UFP layer, and their location is strongly dependent on wind direction. It is not clear in what manner particles age during nighttime transport in the RL. However, as they are decoupled from fresh biogenic emissions and this layer is often drier than the PBL, growth would not always be expected and even shrinking may occur. This means that number concentrations are likely affected by coagulation and diffusion only. In either case, UFP transport to the ground depends on the strength of the thermal convection, which, in turn, depends on the energy input by solar radiation since sunrise, the strength of the inversion layer, and/or a preexisting haze or fine particle load within the surface layer that could reduce or suppress thermal convection. Convective dilution to higher altitudes, with increasing PBL height later in the day, accounts for a further decrease of particle number concentrations in

the whole increasing volume of the PBL (Fig. 1). Once mixed with biogenic emissions, growth occurs as a result of agglomeration of volatile organic compounds (VOC; or ELVOC) (Ehn et al. 2014).

The observation that UFP burst events at field sites occur more frequently in spring than in summer (Dal Maso et al. 2005; Petäjä et al. 2016) is well in line with the more pronounced differences between air and

surface temperatures in springtime, which offer more favorable conditions for thermal convective activity. During the summer months, the nocturnal inversion could be less pronounced because of the higher nighttime surface temperatures, but final mixing-layer depth and thus vertical dilution may be higher (Fig. 1).

EXPERIMENTAL SETUP AND OBSERVATION STRATEGY.

As the emission and modification of anthropogenically generated UFPs takes place in either the PBL or the lower free troposphere (FT) at local to regional scales, we used a highly versatile flying laboratory, with miniaturized state-of-the-art aerosol, air chemistry, and meteorology sensors (Table 1) mounted in instrumentation pods carried by aircraft capable of flying low and

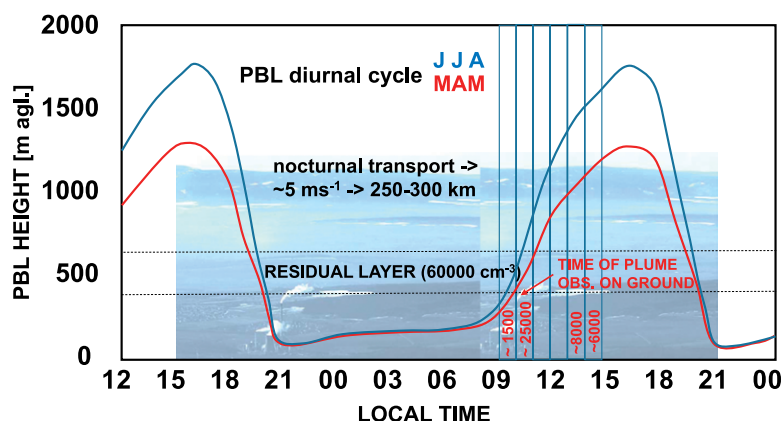


FIG. 1. Temporal development of the planetary boundary layer (PBL) in summer [Jun–Aug (JJA)] and spring [Mar–May (MAM)]. PBL data taken from the ARM Southern Great Plains (SGP) site, Oklahoma (www.arm.gov/capabilities/observatories/sgp), adapted from Liu and Liang (2010). Background picture: Buschhaus power station, Germany. UFP plumes emitted into a ~300-m RL with ~60,000 cm⁻³ and approximated ground concentrations for hourly intervals between 1000 and 1400 local time. UFPs injected into the well-mixed PBL during the day reach the ground after ~15 min; later in the day, full PBL mixing prevents high ground concentrations. More detailed description in the text.

TABLE 1. Airborne campaigns with UFP observations and source apportionment. Campaigns C1–C8 cover regional-scale experiments ~100 km × 100 km, campaigns C9–C13 are long-distance flight missions, and the instruments column omits meteorological sensors—included in all projects. Acidic salt lakes (ASL); marine traffic (MT).

Country	Instrument	Year	Source	Reference
C1 Italy	1 CPC	1998–2000	FFPS, REF	Junkermann et al. (2002)
C2 Ireland	2 CPC	2002	Coastal ponds	O'Dowd et al. (2007)
C3 France	1 CPC	2002	REF*	Junkermann (2005)
C4 Finland	2 CPC	2003	FFPS*, SME	Laaksonen et al. (2008); O'Dowd et al. (2009)
C5 Italy	2 CPC	2004	FFPS*, REF	Laaksonen et al. (2005)
C6 Great Britain	CPC	2003–04	FFPS*	Thiel et al. (2008)
C7 Germany	CPC, SMPS	2007	FFPS	Junkermann et al. (2011a)
C8 Australia (WA)	CPC, SMPS	2006, 2007	ASL	Junkermann et al. (2009)
C9 China	1 CPC	2007, 2009	FFPS	Junkermann et al. (2011b)
C10 Australia (WA)	CPC, SMPS	2011, 2012	ASL/FFPS/SME	Junkermann et al. (2011b)
C11 Australia (Queensland)	CPC, SMPS	2012	FFPS/SME	Junkermann&Hacker (2015)
C12 Germany	CPC, SMPS	2012, 2014	FFPS/REF	Junkermann et al. (2016)
C13 Australia (SA)	CPC, SMPS	2014	FFPS/SME	This study
C14 France/Malta	CPC, SMPS	2012, 2013	FFPS/MT	Mallet et al. (2016)

* Source apportionment from recent reanalysis.

slow but also capable of climbing rapidly into the FT. The instruments, covering aerosols, air chemistry, and meteorology are listed in Table 2. For studies in Australia, the aerosol package was installed in the underwing pods of the Airborne Research Australia (ARA) motorized glider, which is already instrumented for (micro)meteorological measurements (Hacker and Crawford 1999; Hacker et al. 2016) (Fig. 2). Using slow-flying aircraft proved to be a well-matched approach to capturing the spatial scale of UFP events, as well as to achieve the desired spatial resolution given by the temporal resolution of the instrumentation. The comparatively slow-flying speed and simple installation in instrument pods with extremely short inlet lines (between 5 and 30 cm for the aerosol instruments) also helped to avoid sampling problems that are common in larger, faster, and often pressurized aircraft, where samples tend to be constrained to sizes >20 nm, owing to loss processes in the inlet lines (Andreae et al. 2018).

In our study, two aircraft were used, the Karlsruhe Institute of Technology (KIT) microlight (Junkermann 2001) and the ARA motorized glider (Junkermann and Hacker 2015). Typical cruising speed is 25 m s⁻¹ for the microlight and 40 m s⁻¹ for the motorized glider, resulting in a horizontal resolution of 1.5–2.4 km of sampling length for a complete UFP size distribution (2 min) and a 20–40-m resolution for the particle number concentration. Vertically, a 1-s resolution corresponds to less than 5-m altitude change. A real-time display of the sensor values in the cockpit allows immediate adjustment of the flight procedure. For instance, in case of a rapidly changing CPC signal, the aircraft can be held at constant altitude and approximate location until a full size distribution is completed. Overall, the instrumentation ensured a lower detection limit of below 5 nm, several size bins resolving the nucleation mode (<10 nm), and sufficient sensitivity to measure size distributions even in pristine environments.

TABLE 2. Instrumentation package for aerosols, (micro) meteorology, and air chemistry installed in the microlight aircraft (changes for the ARA motorized glider relevant for the current study are shown in the bottom several rows). Accuracy of aerosol size and number instrumentation is within ± 10% (www.grimm-aerosol.de). For a detailed description of the performance of GRIMM CPC and OPS in airborne applications, see Bundke et al. (2015); for the (micro) meteorological instrumentation, see Metzger et al. (2012) and Hacker and Crawford (1999). Internal quality control of the total SMPS counts conducted with an independent CPC. A description of the aethalometer is available online (<https://mageesci.com>). Temperatures are measured within ±0.2°C and ozone within ±3 ppb. (D = particle diameter; SMPS = Scanning Mobility Particle Sizer; OPS = Optical Particle Spectrometer; FSSP = Forward Scattering Spectrometer Probe.)

Parameter	Instrument	Time resolution (s)
Aerosol number concentration $D > 4.5$ nm	Condensation particle counter, GRIMM, CPC4	1
Aerosol size distribution $D = 4.5$ –350 nm	SMPS, GRIMM, 5403	120
Aerosol size distribution $D = 0.3$ –20 μ m	OPS, GRIMM, 1.108	6
Aerosol spectral absorption (seven wavelengths)	Aethalometer Magee, AE42	120
Extinction coef (870 nm), visibility	Nephelometer HSS, Airborne Visibility Meter (AVMIII)	1
3D wind speed and direction/turbulence	Turbulence probe	0.1
Temperature, dewpoint	Chilled mirror, Meteolabor TP3	1
Radiation up- and downwelling	Pyranometer, Licor, LI-200	1
Longwave radiation	Pyrgometer, Kipp & Zonen, CGR4	1
Photolysis rates JO'D and JNO ₂	Actinic flux filter radiometers	1
Surface and sky (cloud base) temperature	Infrared temperature sensors (Optris)	1
Ozone	UV absorption	5

ARA motorized glider

Cloud droplet size distribution	FSSP-100, Droplet Measurement Technologies (DMT), Boulder, CO	1
Meteorology/turbulence	Best aircraft turbulence (BAT) probe	0.1

An SMPS was used since 2006 for the measurement of the complete size distribution from 4.5 nm upward (Table 1) for the following reasons. Fresh gas-to-particle conversion particles (Mohnen and Lodge 1969; Kiang et al. 1973) grow slowly from cluster sizes (~1 nm) into nucleation mode (>5 nm) (Kulmala et al. 2013). UFPs with a size of about 6–10 nm originating from atmospheric GPC (or NPF) should then already be a few hours old with those above 25 nm more than half a day (Kulmala et al. 2013). Direct primary emissions from anthropogenic sources, however, are emitted already in a nucleation size mode of ~6–15 nm (Junkermann et al. 2011a; Brachert et al. 2013; Junkermann and Hacker 2015; see also Fig. 4) and contain only few particles below 5 nm. Size distributions containing both primary emissions and secondary GPC particles are characterized by a broader distribution, an aged Aitken mode, and increased numbers of particles in the lower-size bins. That way, from the shape and modes of the size distribution an approximate particle age can be derived and leads to a considerably more detailed picture than the initial twin CPC approach.

Flight patterns include initial vertical profiles extending from near the ground into the FT to define the height of the PBL, to detect UFPs in the lower FT, and to confirm that the PBL is well mixed and regional-scale (>300 km) horizontal patterns to identify and trace possible sources. Lagrangian flight patterns across plumes from several individual anthropogenic sources at different downwind distances were used to derive particle budgets and to investigate aerosol aging.

Long-distance survey flights in 2012 over Australia (distances of >3,500 km) and in 2012/14 over Germany (>2,000 km) were used to investigate the relative frequency of occurrence of anthropogenic particles, as well as any indications of potential contributions of biogenic-particle-related processes. Biogenic particles from atmospheric gas to particle conversion (nucleation) would be expected, for example, at low to midelevations of the PBL over VOC-emitting forest areas and most likely under sunny conditions (i.e., between midmorning to early afternoon hours). A search for biogenic UFPs would thus require flights between 1000 and 1500 local time and under at least

partially sunny conditions (Baranizadeh et al. 2014). In contrast, anthropogenic primary emissions from continuously operating aerosol sources should be independent of the time of day. This notion was confirmed in Junkermann and Hacker (2015) for flights downwind of the 750-MW Kogan Creek power station in Queensland, Australia, over 1 h around sunset (SS) (takeoff 30 min before SS and landing 30 min after SS) and in the late morning the next day, with particle emissions of 3×10^{18} particles s^{-1} in both cases (Junkermann and Hacker 2015).

From an operational perspective, and to adjust and optimize flight strategy and flight patterns to the actual meteorological and environmental conditions, the real-time data display in the aircraft and



FIG. 2. Two aircraft, one set of aerosol instruments. (top) The KIT microlight aircraft with aerosol pod (15 kg) mounted at the left-hand side of the fuselage, also showing in the insert the in situ display in the cockpit and the aerosol and cloud droplet instrumentation [CPC, Optical Particle Spectrometer (OPC), SMPS, Forward Scattering Spectrometer Probe (FSSP); Table I]. (bottom) ARA (left) motorized glider and (right) instrumentation pod. The KIT aerosol pod fits into one of the motorized glider’s underwing pods, shown here with the additional FSSP-100 for cloud droplet size distribution measurements during campaign C8 in 2006/07. Radiation sensors on the microlight are mounted on gimballed $\pm 0.2^\circ$ platforms above the wing.

visual clues observed by the scientist/pilots were essential decision-making tools. Having the freedom to fly the research aircraft mostly in noncontrolled airspace under visual flight rules (VFR) enabled rapid changes of the flight strategy in response to real-time observations. This flexibility, and the comparatively low flying altitude above ground, is usually not feasible for larger aircraft (Hamburger et al. 2012).

RESULTS. Results from multiple airborne campaigns flown since 1998 over various European countries as well as Australia and China (see Table 1) form the basis for the current study. The following paragraphs present key findings from these campaigns that are then combined to form a novel overall interpretation and explanation of the spatial and temporal UFP occurrence within the lower troposphere. For the campaigns C1 to C6 in Table 1, a twin CPC approach with different size cutoffs, 3 and 10 nm, was used to trace UFPs over regional-scale ranges of up to 150 km by 150 km and in the vertical from ~10 to 3,000 m AGL. Local-scale (<5 km) UFP events were observed over individual coastal basins at the Irish west coast at Mace Head, Ireland (campaign C2), most likely attributable to biogenic sources (O'Dowd et al. 2007). High UFP concentrations over the boreal forests at Hyytiälä, Finland, in 2003 (campaign C4) and concurrent low concentrations over the embedded (ice covered) lakes in the area (O'Dowd et al. 2009) suggested a link between land surface properties, albedo, surface roughness, local biogenic emissions, and UFP spatial distribution. However, a clear source attribution was not successful with the limited instrumentation applied in these campaigns (O'Dowd et al. 2007, 2009; Laaksonen et al. 2008) (campaigns C2, C4, and C5). Anthropogenic sources of UFPs within the nucleation mode (4–10 nm) from fossil fuel burning were clearly identified for the first time as major emission in 2007 in a plume study downwind of the city of Karlsruhe, Germany. A coal-fired power station and a large refinery (REF) there dominated the city plume (Junkermann et al. 2011a; campaign C7). Similar industrial installations are located in the Italian Po Valley, a region that we investigated already in 2004 (campaign C5) without being able to identify the UFP sources. The conditions for atmospheric secondary particle formation were quite different from the boreal forest in Finland, with higher pollution levels and higher UV radiation but most likely less biogenic emissions over the agricultural land in early spring season. Also, the onset of UFP events was delayed until about noon with respect to Finland, despite the higher UV radiation levels (Hamed et al. 2007).

Using a more detailed Hybrid Single-Particle Lagrangian Integrated Trajectory model (HYSPLIT; Draxler and Rolph 2013) analysis for the case study of Laaksonen et al. (2005), the UFP events could be reassigned to a plume originating from the Mestre industrial complex in Italy about 6 h upwind under changing wind conditions.

In 2006/07 we were able to identify, for the first (and so far only) time, a local clearly non-fossil fuel source of nucleation mode particles in Western Australia (WA). Interestingly, these UFPs were found not above the forest but over the adjacent agricultural area with embedded salt lakes. These lakes were identified as the particle sources and attributable to a change in lake chemistry following deforestation decades ago (Junkermann et al. 2009; Kamilli et al. 2016) (campaigns C9 and C10). This remained the only case in about 1,200 flight hours spanning more than 15 years of our airborne research where a natural source significantly contributed to the regional budget of UFPs at a similar magnitude as anthropogenic sources. Similar to the missing nucleation mode particles in (above canopy) measurements over the Amazon (Fan et al. 2018; Andreae et al. 2018), we never found any signatures of atmospheric nucleation over the forested areas of Australia (Junkermann et al. 2009; Junkermann and Hacker 2015).

Enhanced UFP number concentrations were observed several times over the grasslands of Inner Mongolia (China) during a research project focusing on turbulent fluxes of energy and water vapor (campaign C8; Junkermann et al. 2011b). Because of legal limitations to import a radioactive source for the SMPS into China, it was only possible to use one CPC combined with sophisticated turbulence and meteorology instrumentation (Metzger et al. 2013). In one instance, while flying a 3 km by 5 km rectangular pattern at 500 m AGL, a local UFP event was observed under changing wind direction in a well-mixed boundary layer (up to 2,000 m AGL). A HYSPLIT analysis clearly related the origin of the plume to a power station at Xilinhot, China (see Fig. 3), 65 km to the north of the flight location. Over a 3-h period, the particle number concentration changed in response to this plume sweeping over the area because of a gradually backing wind direction. It increased from 1,000 cm⁻³ background to 40,000 cm⁻³ concurrently with a marked increase of surface temperature from 25° up to 45°C, well above the boundary layer temperature at 500 m of nearly constant ~19°–20°C. The particle number concentration peaked after ~90 min and then decreased again to background, displaying a signature very

similar to UFP events observed in ground-based events elsewhere.

The most important overall finding for a better understanding of the observed patterns in UFP distributions was that, with the exception of Mace Head (O'Dowd et al. 2007) and Western Australia (Junkermann et al. 2009), all of our pronounced UFP event observations could without doubt be traced back to a limited number of large, modern, so-called clean, fossil fuel-burning sources, even in the presence of big-city plumes (Bonn et al. 2016). Most importantly, the magnitudes of these UFP events could not be explained plausibly without recognizing atmospheric advection to be the essential mechanism. It was possible to confirm this for every single case studied.

The location and technical description of most of these anthropogenic sources is well documented worldwide (<http://endcoal.org/tracker>). With a major nucleation mode between 5 and 15 nm and only minor particle concentrations in the lowest size bins, the size spectrum of the emitted particles matches the size distributions initially observed during ground-

based UFP events well (Junkermann et al. 2011a, 2016; Junkermann and Hacker 2015).

Airborne aerosol studies in the seventies followed visible plumes for several hundreds of kilometers (Whitby et al. 1978; Pueschel and Van Valin 1978; Ayers et al. 1979; Hobbs et al. 1980). These plumes contained both fine and ultrafine particles and were thus simple to track. The invisible plumes of today, however, which lack significant number concentrations of visible fine particles but contain larger concentrations of UFPs, are more difficult to track but cover similar distances. In a similar approach to our investigations, but without using a size distribution measurement, Bigg and Turvey (1978) found enhanced particle number concentrations 160 km downwind of the city of Perth, speculatively at the time thought to be associated with urban and port emissions. In a later publication they recognized that the coal-fired Muja power station in Australia ~180 km farther to the south may have contributed as a possible source to their measurements (Bigg et al. 2015). In the present study, the relevance of the Muja power

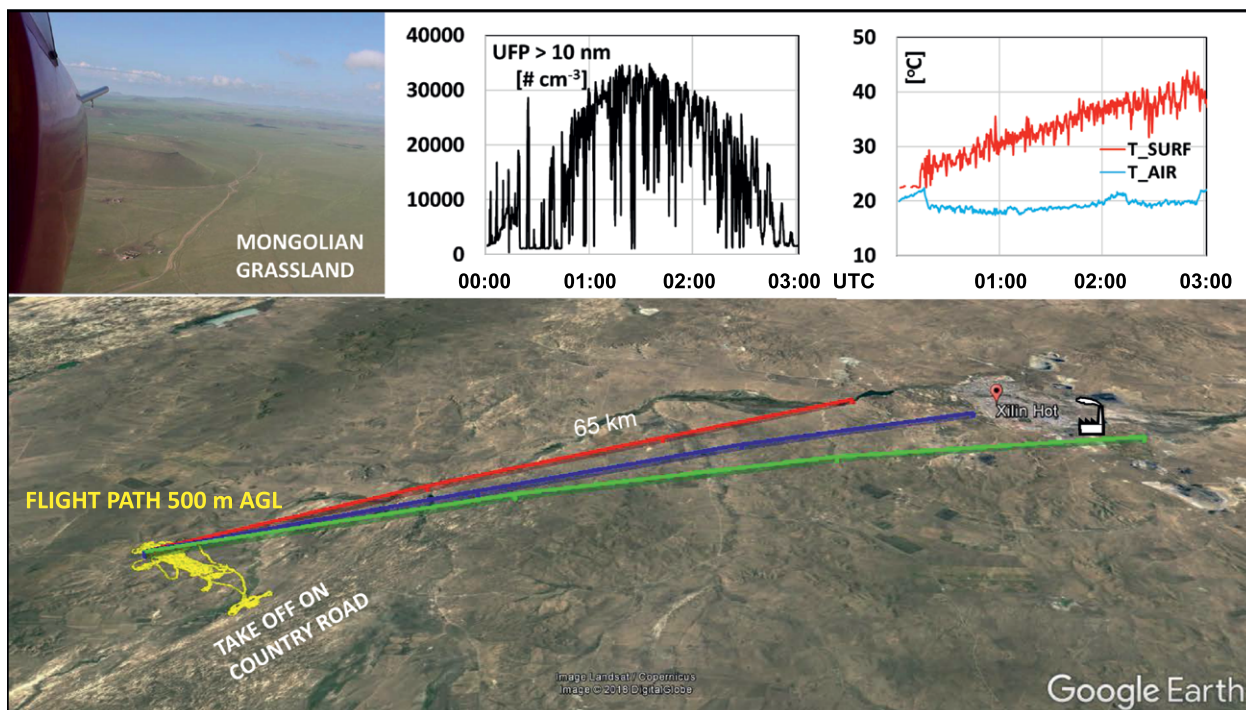


FIG. 3. UFP burst observed on the morning of 3 Jul 2009 over the grasslands of Inner Mongolia (campaign C9); local flight at altitude 1500 m AGL; local time is UTC plus 8 h. (top left) Forward view from the aircraft. (top center) Time series of UFP > 10 nm. (top right) Surface temperature rising from 24° to 39°C (red); air temperature at 500 m AGL remains near constant at ~19°C (blue). Temperatures indicate fully mixed boundary layer with depth >2,000 m (from HYSPLIT). The 3-h back trajectories indicate changing wind direction from the Xilinhot area power station to the east; lines show HYSPLIT trajectories at 2-h intervals, before (green), at maximum (blue), and after plume passage (red). Flight track of the aircraft is shown in yellow.

station was confirmed for this case by HYSPLIT (not shown).

Figure 4 (top panel) shows two contrasting cases of power station emissions, observed in 2014 close to the Polish border (campaign C12), illustrating the impact of daytime versus nighttime meteorology and of clean versus polluted (hazy) PBL conditions, and the effects of horizontal transport and convective vertical mixing. The 8 Jun flight (yellow and brown bars), discussed in more detail in Junkermann et al. (2016), was flown in thermal convective conditions and moderate pollution. The 8 Jun data show two transects (south–north and north–south) under southwesterly winds and ~1-h downwind advection time from the power stations along the Polish border, with emissions into a well-mixed turbulent boundary layer (up to 1,100 m AGL) and surface temperatures well above the threshold for thermal convection. A source strength of $1.5\text{--}2.5 \times 10^{18}$ particles per second for both of the southern power stations was estimated, similar to the emission rates of the Karlsruhe power station (Junkermann et al. 2011a) or Kogan Creek, Queensland (Junkermann and Hacker 2015). On 10 Jun (gray and blue bars), under stable stratified conditions, the high PBL particle load suppressed most of the solar radiation reaching the ground, and surface temperatures accordingly stayed well below the threshold required for initiation of convection (Table 3). In the bottom

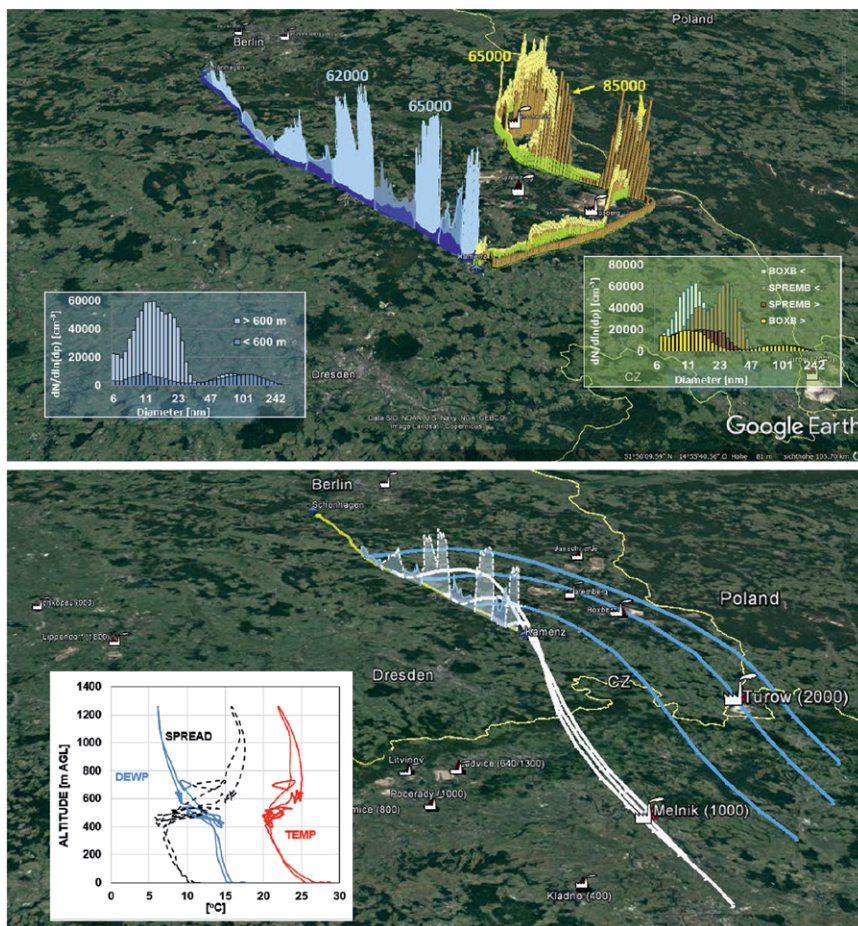


FIG. 4. (top) UFP plumes at the German–Polish border originating from power stations Spremberg, Boxberg, and Jänschwalde, Germany, and Melnik, Czech Republic, under well-mixed moderately polluted and stable stratified heavily polluted conditions, 8 (yellow and brown) and 10 Jun (blue and gray) 2014 (campaign I2). Conditions on 8 Jun included southwesterly winds and well-mixed PBL up to >1,100 m AGL; main image shows particle number concentrations along flight path, max of 85,000 cm^{-3} with PM_{10} 3–4 $\mu\text{g m}^{-3}$ (green; not to scale) BC 300–500 ng m^{-3} (not shown). Yellow and light brown colors for individual plume cross sections and corresponding size distributions in the plumes of Spremberg and Boxberg (corresponding colors). On 10 Jun, there were stable conditions with clean RL (light blue) above a hazy and polluted PBL (dark gray) and southerly to southeasterly winds. Above, in the RL: (PM_{10} ; dark blue; 2–4 $\mu\text{g m}^{-3}$; not to scale) low BC (300–500 ng m^{-3}) but high nucleation mode UFP concentrations (max of 65,000 cm^{-3}). PBL high fine particulate concentrations (dark blue; PM_{10} 10–25 $\mu\text{g m}^{-3}$; not to scale), visibility reduction to <15 km and high BC (up to 2000 ng m^{-3}) but low UFP concentrations (max of 12,000 cm^{-3}) in the Turow power station plume as listed in Table 3. (bottom) Plumes from power stations Turow and Melnik and 15-h HYSPLIT back trajectories for 10 Jun, PBL air (<450 m AGL; blue) and RL (>550 m AGL; white). Insert shows temp, dewpoint (DP), and spread (temp minus DP) profiles for 10 Jun illustrate the stable stratification and the dry RL.

panel of Fig. 4, the 10 Jun data are combined with 15-h HYSPLIT back trajectories for the planetary boundary and the early morning RL above 550 m between Dresden and Berlin, Germany. The flight

altitude was changed several times to cover 1) a highly polluted hazy surface layer and 2) an approximately 400-m-deep clear RL above, separated by a strong (~5°C) inversion at ~500 m AGL (Fig. 4), with a further climb into the FT at the end of the flight pattern. Airmass characteristics for the PBL and the

RL and FT, respectively, are summarized for both days in Table 3. In situ winds from the aircraft on 10 Jun were southeasterly but changed significantly within the few hours before the flight (see also the HYSPLIT trajectories). HYSPLIT analysis suggests that the high particle number concentrations in the

TABLE 3. Aerosol and meteorological parameters on 8 and 10 Jun 2014 within the PBL, RL, and above (FT).

Parameter	8 Jun		10 Jun	
	PBL	FT	PBL	RL
(Flight) Altitude AGL (m)	~500	>1,200	<500	>650
Number concentration (cm ⁻³)	6,000–85,000	~3,500	6,000–15,000	3,000–65,000
PM ₁₀ (μg m ⁻³)	3–4	~2	10–25	2–4
BC (ng m ⁻³)	300–500	~200	1,500–2,000	200–400
Ozone (ppb)	78	80	32	48
Temperature; dewpoint (°C)	27; 9–12	24; 0–2	21; 14	25; 10
Potential temperature (°C)	32	34	25	32
Surface temperature (°C)	28–40	28–40	21	21
Visibility (km)	>80	>150	10–20	>80

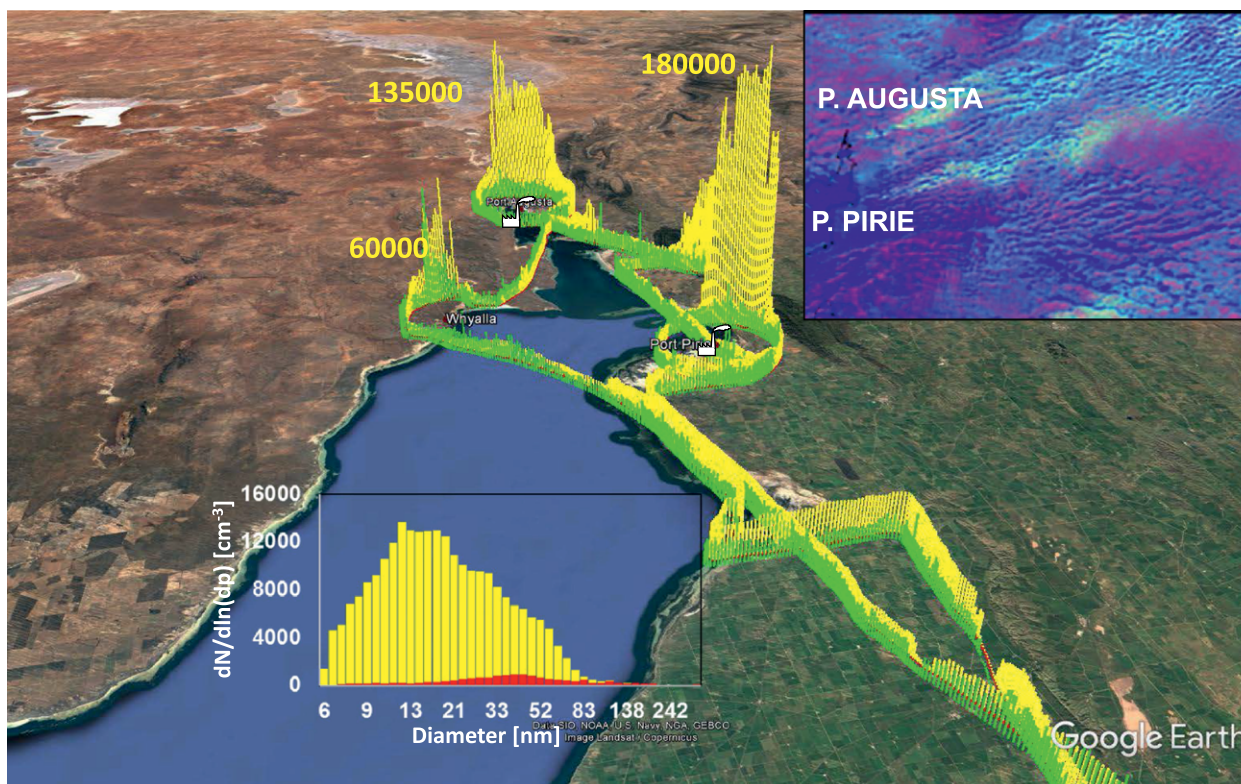


FIG. 5. Particle number concentrations (yellow) and fine particles >300 nm (green) within the PBL 400–600 m AGL north of Adelaide, Australia, 14 Oct 2014 (campaign I3) with south to southwesterly winds. Graph insert: particle size distributions within (yellow) and outside (red) the plume of Port Pirie from ground-based (vehicle based) measurements 70 km downwind. The satellite picture insert shows the corresponding plume of cloud droplets with decreased droplet sizes, plume width about 60 km after 300 km of transport. [Insert courtesy of Daniel Rosenfeld, Hebrew University, Tel Aviv, Israel; see also Rosenfeld (2000).]

upper layer are due to emissions into the evening or nocturnal RL (~100 m AGL) from the Czech “clean” power station Melnik located 120 km upwind. The lower surface layer below 500 m AGL in Fig. 4 was, according to HYSPLIT, affected by the “dirty” power station Turow on the Polish side of the border, featuring the typical composition of unfiltered emissions with high concentrations of particulate matter with diameters of 2.5 and 10 μm or less ($\text{PM}_{2.5}$ and PM_{10} , respectively) and of black carbon (BC), as well as low ozone values (Table 3). The flight results were not conducive to derive particle budgets similar to the previous days, as the plumes were not covered by the flight to their full extent. However, they resulted in a case study of the vertical stratiform layers in the early morning lower troposphere and confirmed nighttime transport in the RL.

To illustrate the impact emissions can have on meteorological parameters, Fig. 5 shows the plume characteristics of two large UFP sources located north of Adelaide, South Australia (SA), in October 2014: the smelter (SME) at Port Pirie and the Port Augusta power station (campaign C13). At a distance of 10 km from the stacks the two plumes contained more than 180,000 and 130,000 particles per cubic centimeter, respectively. The satellite image insert (from 1997; Rosenfeld 2000) shows for the same southwesterly wind direction the cloud modification with reduced droplet sizes in stratiform clouds over distances of >1,000 km. The second insert shows SMPS data from the two UFP sources measured along a 40-km road at a distance of ~70–100 km, after approximately 2–3-h advection time downwind.

It was possible to track these plumes over sparsely populated inland areas of Australia over 3 days and more than 1,200 km during a long-distance survey from Adelaide to Chinchilla, Queensland (Junker and Hacker 2015). Secondary GPC changed the size

distribution within this plume during days 2 and 3. While aging shifted the initial aerosol mode to larger sizes, fresh particles from GPC in the sulfur-containing plume (Mohnen and Lodge 1969; Kiang et al. 1973) refilled the smallest-size bins but without any known sulfur emitter less than 400 km upwind. All back trajectories indicate Port Pirie and Port Augusta as the most likely sulfur sources.

Figure 6 shows such power-station-emission-related continental cloud modification, as detected from satellite for an area of the Czech and German power stations (cf. also Fig. 4).

Our airborne experiments resulted in a clear picture of major anthropogenic sources of primary nucleation mode particles, predominately from fossil fuel burning. We were also able to quantify these emissions, based on measurements in Europe, Australia, and China, data urgently needed for updated emission scenarios (Paasonen et al. 2016; Xausa et al. 2018).

SUMMARY AND CONCLUSIONS. Based on airborne experiments using fully instrumented small environmental research aircraft, the impact of horizontal transport and vertical convective mixing

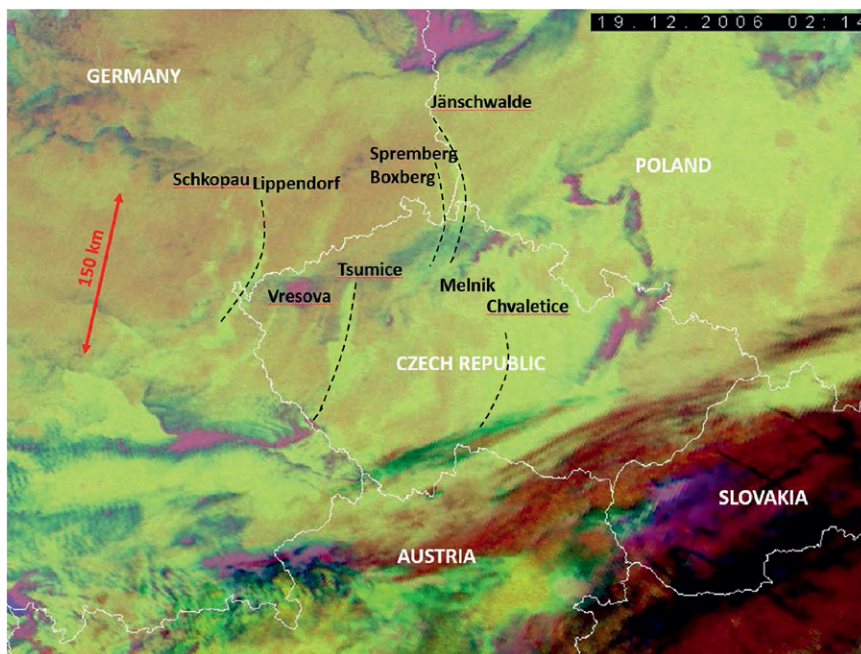


Fig. 6. Power station “tracks” showing brighter clouds observed from space within a stratiform cloud deck over Germany, Poland, and the Czech Republic. The plumes under northerly to northeasterly winds, less clear compared to ship tracks over a dark sea surface but marked with dotted lines, originate from the same power stations investigated in more detail in Jun 2012 and 2014 (Fig. 4; campaign 12). Individual power stations can be identified. (Image courtesy of Daniel Rosenfeld, Hebrew University, Tel Aviv, Israel.)

on the UFP three-dimensional distribution was investigated in local, regional, and long-distance surveys. Size distributions, number concentrations, in situ meteorology (3D wind, temperature, and dewpoint), and HYSPLIT back trajectories allowed us to identify the most persistent UFP sources in the PBL—modern-technology fossil fuel-burning power stations (FFPS), refineries, and smelters—and even to quantify their emissions as particle number emission factors proportional to the installed power. Number concentrations in the plumes from these sources exceeded background values by up to two orders of magnitude. These continuous elevated single-point UFP emitters are perfect emission sources for detailed case studies of meteorological transport, thermal convection, and vertical mixing processes.

Synoptic transport (horizontal) and thermal convection (vertical) (Georgii 1956; Stull 1988) were identified to control the three-dimensional distribution of these primary emitted UFPs over hundreds of kilometers. Diurnal meteorological patterns affect stratification, vertical mixing, and the morning breakup of nighttime stratification. The size, number, and spatial and temporal UFP distributions observed at ground-based rural and urban field sites during all of our field campaigns are well in agreement with such a meteorology-controlled redistribution and diurnal vertical mixing of anthropogenic UFPs. The increasing number of observations of short-duration UFP events within the last decades, compared to observations before 1990, coincides with increases of the number of modern “clean” coal-fired power stations in operation worldwide. The recent changes in anthropogenic flue-gas-cleaning technology suppressing fine particles and NO_x emissions lead toward a dramatic increase in nucleation mode particles (Junkermann et al. 2011b; Li et al. 2017) and affect rural clean as well as polluted environments, even including megacities (Laaksonen et al. 2005, 2008; Birmili et al. 2013; Pan et al. 2016; Kulmala 2017). Taking transport of primary UFPs from upwind fossil fuel-burning sources into account, recently postulated hypothetical elevated sources for ultrafine particles (Wehner et al. 2010; Crippa et al. 2012; Platìs et al. 2015; Andreae et al. 2018) are no longer needed to understand observations. Our results also show that the long-distance origin of the air mass investigated is often less important than the contribution of pollution picked up during transport.

Not only do meteorological processes modify the aerosol distributions, but the ultrafine aerosols also

affect meteorological processes, mainly through aerosol–cloud interactions. In a first step, additional CCN reduce the size of cloud droplets and increase the time necessary for raindrop formation. This has consequences for the spatial and temporal distribution of liquid cloud water, water vapor (latent heat), rainfall, and lightning (Thornton et al. 2017). Furthermore, this might also result in longer drought periods and the frequency and intensity of torrential rain (Rosenfeld et al. 2011; Fan et al. 2018). As the underlying physical processes are highly nonlinear and subject to several feedback loops between ultrafine and fine particles, cloud droplets and their size distributions, water vapor, radiation, and aerosol removal processes through rainout and deposition, a detailed investigation of the secondary cloud processes requires sophisticated modeling efforts that include updated emission scenarios for fossil fuel power station emissions (Paasonen et al. 2016; Xausa et al. 2018). Model calculations for Western Australia (Heinzeller et al. 2016) confirmed that the impact of realistic UFP emissions in terms of size and order of magnitude from single anthropogenic sources is well in agreement with the observed changes in regional-scale rainfall.

Further targeted numerical simulations that include detailed aerosol and cloud microphysics are required to better understand these complex processes combined with further airborne and ground-based measurements. Experimental quantification of the contribution of fossil fuel-burning emitters to the regional budget of UFPs and CCN could be shown to be possible using suitably equipped small environmental research aircraft with miniaturized instrumentation. Airborne measurements as presented here provide the required input data concerning source strength (emission factors) and size distributions to improve current and future emission scenarios for such simulations.

ACKNOWLEDGMENTS. The flight campaign in Inner Mongolia was funded by the German Research Foundation, research group FOR 536 MAGIM, “Matter fluxes in grasslands of Inner Mongolia as influenced by stocking rate,” and the National Natural Science Foundation of China, Grant 41021004. Survey flights in Australia were supported by the German Federal Ministry for Education and Research, Grant AUS 10/031, and the European Commission supported the QUEST project (EVK2-CT2001-00127). The ARA Research Aircraft was donated by the late Ms. Joyce Schulz of Glen Osmond. ARA is supported by the Hackett Foundation in Adelaide.

REFERENCES

- Aitken, J., 1889: On the number of dust particles in the atmosphere. *Trans. Roy. Soc. Edinburgh*, **35**, 1–19, <https://doi.org/10.1017/S0080456800017592>.
- , 1894: On the number of dust particles in the atmosphere of certain places in Great Britain and on the continent, with remarks on the relation between the amount of dust and meteorological phenomena. *Trans. Roy. Soc. Edinburgh*, **37**, 621–693, <https://doi.org/10.1017/S0080456800032762>.
- Albrecht, B. A., 1989: Aerosols, cloud microphysics, and fractional cloudiness. *Science*, **245**, 1227–1230, <https://doi.org/10.1126/science.245.4923.1227>.
- Andreae, M. O., 2009: Correlation between cloud condensation nuclei concentration and aerosol optical thickness in remote and polluted regions. *Atmos. Chem. Phys.*, **9**, 543–556, <https://doi.org/10.5194/acp-9-543-2009>.
- , and Coauthors, 2018: Aerosol characteristics and particle production in the upper troposphere over the Amazon Basin. *Atmos. Chem. Phys.*, **18**, 921–961, <https://doi.org/10.5194/acp-18-921-2018>.
- Ayers, G. P., E. K. Bigg, and D. E. Turvey, 1979: Aitken particle and cloud condensation nucleus fluxes in the plume from an isolated industrial source. *J. Appl. Meteor.*, **18**, 449–459, [https://doi.org/10.1175/1520-0450\(1979\)018<0449:APACCN>2.0.CO;2](https://doi.org/10.1175/1520-0450(1979)018<0449:APACCN>2.0.CO;2).
- Bae, M.-S., J. J. Schwab, O. Hogrefe, B. P. Frank, G. G. Lala, and K. L. Demerjian, 2010: Characteristics of size distributions at urban and rural locations in New York. *Atmos. Chem. Phys.*, **10**, 4521–4535, <https://doi.org/10.5194/acp-10-4521-2010>.
- Baranizadeh, E., and Coauthors, 2014: The effect of cloudiness on new-particle formation: Investigation of radiation levels. *Boreal Environ. Res.*, **19** (Suppl.), 343–354.
- Bigg, E. K., and D. E. Turvey, 1978: Sources of atmospheric particles over Australia. *Atmos. Environ.*, **12**, 1643–1655, [https://doi.org/10.1016/0004-6981\(78\)90313-X](https://doi.org/10.1016/0004-6981(78)90313-X).
- , G. P. Ayers, and D. E. Turvey, 1978: Measurement of the dispersion of a smoke plume at large distances from the source. *Atmos. Environ.*, **12**, 1815–1818, [https://doi.org/10.1016/0004-6981\(78\)90340-2](https://doi.org/10.1016/0004-6981(78)90340-2).
- , S. Soubeyrand, and C. E. Morris, 2015: Persistent after-effects of heavy rain on concentrations of ice nuclei and rainfall suggest a biological cause. *Atmos. Chem. Phys.*, **15**, 2313–2326, <https://doi.org/10.5194/acp-15-2313-2015>.
- Birmili, W., and Coauthors, 2013: Variability of aerosol particles in the urban atmosphere of Dresden (Germany): Effects of spatial scale and particle size. *Meteor. Z.*, **22**, 195–211, <https://doi.org/10.1127/0941-2948/2013/0395>.
- Bister, M., and M. Kulmala, 2011: Anthropogenic aerosols may have increased upper troposphere humidity in the 20th century. *Atmos. Chem. Phys.*, **11**, 4577–4586, <https://doi.org/10.5194/acp-11-4577-2011>.
- Bonn, B., and Coauthors, 2016: BAERLIN2014—The influence of land surface types on and the horizontal heterogeneity of air pollutant levels in Berlin. *Atmos. Chem. Phys.*, **16**, 7785–7811, <https://doi.org/10.5194/acp-16-7785-2016>.
- Brachert, L., T. Kochenburger, and K. Schaber, 2013: Facing the sulfuric acid aerosol problem in flue gas cleaning: Pilot plant experiments and simulation. *Aerosol Sci. Technol.*, **47**, 1083–1091, <https://doi.org/10.1080/02786826.2013.824549>.
- Bundke, U., and Coauthors, 2015: The IAGOS-CORE aerosol package: Instrument design, operation and performance for continuous measurement aboard in-service aircraft. *Tellus*, **67B**, 28339, <https://doi.org/10.3402/tellusb.v67.28339>.
- Buzorius, G., U. Rannik, D. Nilsson, and M. Kulmala, 2001: Vertical fluxes and micrometeorology during aerosol particle formation events. *Tellus*, **53B**, 394–405, <https://doi.org/10.3402/tellusb.v53i4.16612>.
- Coulier, M., 1875: Note sur une nouvelle propriété de l'air. *J. Pharm. Chem.*, **4**, 22–24.
- Crippa, P., T. Petäjä, H. Korhonen, G. S. El Afandi, and S. C. Pryor, 2012: Evidence of an elevated source of nucleation based on model simulations and data from the NIFTy experiment. *Atmos. Chem. Phys.*, **12**, 8021–8036, <https://doi.org/10.5194/acp-12-8021-2012>.
- Crumeyrolle, S., and Coauthors, 2010: New particle formation events measured on board the ATR-42 aircraft during the EUCAARI campaign. *Atmos. Chem. Phys.*, **10**, 6721–6735, <https://doi.org/10.5194/acp-10-6721-2010>.
- Dall'Osto, M., and Coauthors, 2018: Novel insights on new particle formation derived from a pan-European observing system. *Sci. Rep.*, **8**, 1482, <https://doi.org/10.1038/s41598-017-17343-9>.
- Dal Maso, M., and Coauthors, 2005: Formation and growth of fresh atmospheric aerosols: Eight years of aerosol size distribution data from SMEAR II, Hyytiälä, Finland. *Boreal Environ. Res.*, **10**, 323–336.
- Draxler, R. R., and G. D. Rolph, 2013: HYSPLIT. NOAA/Air Resources Laboratory, <http://ready.arl.noaa.gov/HYSPLIT.php>.
- Ehn, M., and Coauthors, 2014: A large source of low-volatility secondary organic aerosol. *Nature*, **506**, 476–479, <https://doi.org/10.1038/nature13032>.
- Fan, J., and Coauthors, 2018: Substantial convection and precipitation enhancements by ultrafine aerosol

- particles. *Science*, **359**, 411–418, <https://doi.org/10.1126/science.aan8461>.
- Georgii, H. W., 1956: *Flugmeteorologie*. 2nd ed. Akademische Verlagsgesellschaft, 332 pp.
- Hacker, J. M., and T. Crawford, 1999: The BAT-Probe: The ultimate tool to measure turbulence from any kind of aircraft (or sailplane). *Tech. Soaring*, **23**, 43–47.
- , and Coauthors, 2016: Using airborne technology to quantify and apportion emissions of CH₄, N₂O and NH₃ from feedlots. *Anim. Prod. Sci.*, **56**, 190–203, <https://doi.org/10.1071/AN15513>.
- Hamburger, T., and Coauthors, 2012: Airborne observations of aerosol microphysical properties and particle ageing processes in the troposphere above Europe. *Atmos. Chem. Phys.*, **12**, 11 533–11 554, <https://doi.org/10.5194/acp-12-11533-2012>.
- Hamed, A., and Coauthors, 2007: Nucleation and growth of new particles in Po Valley, Italy. *Atmos. Chem. Phys.*, **7**, 355–376, <https://doi.org/10.5194/acp-7-355-2007>.
- Heintzenberg, J., B. Wehner, and W. Birmili, 2007: “How to find bananas in the atmospheric aerosol”: New approach for analyzing atmospheric nucleation and growth events. *Tellus*, **59B**, 273–282, <https://doi.org/10.1111/j.1600-0889.2007.00249.x>.
- , P. Tunved, M. Galí, and C. Leck, 2017: New particle formation in the Svalbard region 2006–2015. *Atmos. Chem. Phys.*, **17**, 6153–6175, <https://doi.org/10.5194/acp-17-6153-2017>.
- Heinzeller, D., W. Junkermann, and H. Kunstmann, 2016: Anthropogenic aerosol emissions and rainfall decline in southwestern Australia: Coincidence or causality. *J. Climate*, **29**, 8471–8493, <https://doi.org/10.1175/JCLI-D-16-0082.1>.
- Held, A., A. Nowak, W. Birmili, A. Wiedensohler, R. Forkel, and O. Klemm, 2004: Observations of particle formation and growth in a mountainous forest region in central Europe. *J. Geophys. Res.*, **109**, D23204, <https://doi.org/10.1029/2004JD005346>.
- Hobbs, P. V., J. L. Stith, and L. F. Radke, 1980: Cloud active nuclei from coal-fired power plants and their interactions with clouds. *J. Appl. Meteor.*, **19**, 439–451, [https://doi.org/10.1175/1520-0450\(1980\)019<0439:CANFCF>2.0.CO;2](https://doi.org/10.1175/1520-0450(1980)019<0439:CANFCF>2.0.CO;2).
- Hogan, A., W. Winters, and S. Barnard, 1981: Photo electric nucleus counters for aerosol climatology. *J. Aerosol Sci.*, **12**, 477–489, [https://doi.org/10.1016/0021-8502\(81\)90051-3](https://doi.org/10.1016/0021-8502(81)90051-3).
- Junkermann, W., 2001: An ultralight aircraft as platform for research in the lower troposphere: System performance and first results from radiation transfer studies in stratiform aerosol layers and broken cloud conditions. *J. Atmos. Oceanic Technol.*, **18**, 934–946, [https://doi.org/10.1175/1520-0426\(2001\)018<0934:AUAAPF>2.0.CO;2](https://doi.org/10.1175/1520-0426(2001)018<0934:AUAAPF>2.0.CO;2).
- , 2005: The actinic UV-radiation budget during the ESCOMPTE campaign 2001: Results of airborne measurements with the microlight research aircraft D-MIFU. *Atmos. Res.*, **74**, 461–475, <https://doi.org/10.1016/j.atmosres.2004.06.009>.
- , and J. M. Hacker, 2015: Ultrafine particles over eastern Australia: An airborne survey. *Tellus*, **67B**, 25308, <https://doi.org/10.3402/tellusb.v67.25308>.
- , and Coauthors, 2002: Actinic radiation and photolysis processes in the lower troposphere: Effect of clouds and aerosols. *J. Atmos. Chem.*, **42**, 413–441, <https://doi.org/10.1023/A:1015774415983>.
- , J. Hacker, T. Lyons, and U. Nair, 2009: Land use change suppresses precipitation. *Atmos. Chem. Phys.*, **9**, 6531–6539, <https://doi.org/10.5194/acp-9-6531-2009>.
- , R. Hagemann, and B. Vogel, 2011a: Nucleation in the Karlsruhe plume during the COPS/TRACKS-Lagrange experiment. *Quart. J. Roy. Meteor. Soc.*, **137**, 267–274, <https://doi.org/10.1002/qj.753>.
- , B. Vogel, and M. A. Sutton, 2011b: The climate penalty for clean fossil fuel combustion. *Atmos. Chem. Phys.*, **11**, 12 917–12 924, <https://doi.org/10.5194/acp-11-12917-2011>.
- , —, and M. Bangert, 2016: Ultrafine particles over Germany—An aerial survey. *Tellus*, **68B**, 29250, <https://doi.org/10.3402/tellusb.v68.29250>.
- Kamilli, K. A., and Coauthors, 2016: How salt lakes affect atmospheric new particle formation: A case study in western Australia. *Sci. Total Environ.*, **573**, 985–995, <https://doi.org/10.1016/j.scitotenv.2016.08.058>.
- Kiang, C. S., D. Stauffer, V. A. Mohnen, J. Bricard, and D. Vigla, 1973: Heteromolecular nucleation theory applied to gas to particle conversion. *Atmos. Environ.*, **7**, 1279–1283, [https://doi.org/10.1016/0004-6981\(73\)90137-6](https://doi.org/10.1016/0004-6981(73)90137-6).
- Kontkanen, J., and Coauthors, 2017: Measurements of sub-32 nm particles using a particle size magnifier in different environments: From clean mountain top to polluted megacities. *Atmos. Chem. Phys.*, **17**, 2163–2187, <https://doi.org/10.5194/acp-17-2163-2017>.
- Kulmala, M., and V. M. Kerminen, 2008: On the formation and growth of atmospheric nanoparticles. *Atmos. Res.*, **90**, 132–150, <https://doi.org/10.1016/j.atmosres.2008.01.005>.
- , and Coauthors, 2004: Formation and growth rates of ultrafine atmospheric particles: A review of observations. *J. Aerosol Sci.*, **35**, 143–176, <https://doi.org/10.1016/j.jaerosci.2003.10.003>.

- , and Coauthors, 2011: General overview: European Integrated Project on Aerosol Cloud Climate and Air Quality Interactions (EUCAARI)—Integrating aerosol research from nano to global scales. *Atmos. Chem. Phys.*, **11**, 13 061–13 143, <https://doi.org/10.5194/acp-11-13061-2011>.
- , and Coauthors, 2013: Direct observations of atmospheric aerosol nucleation. *Science*, **339**, 943–946, <https://doi.org/10.1126/science.1227385>.
- , and Coauthors, 2017: Atmospheric gas-to-particle conversion: Why NPF events are observed in megacities. *Faraday Discuss.*, **200**, 271–288, <https://doi.org/10.1039/C6FD00257A>.
- Laaksonen, A., and Coauthors, 2005: Cloud condensation nucleus production from nucleation events at a highly polluted region. *Geophys. Res. Lett.*, **32**, L06812, <https://doi.org/10.1029/2004GL022092>.
- , and Coauthors, 2008: The role of VOC oxidation products in continental new particle formation. *Atmos. Chem. Phys.*, **8**, 2657–2665, <https://doi.org/10.5194/acp-8-2657-2008>.
- Landsberg, H. 1938: Atmospheric condensation nuclei. *Gerlands Beiträge zur Geophysik: Ergebnisse der Kosmischen Physik III*, M. B. H. Leipzig, Ed., Akademische Verlagsgesellschaft, 155–252.
- Latham, J., and Coauthors, 2008: Global temperature stabilization via controlled albedo enhancement of low-level maritime clouds. *Philos. Trans. Roy. Soc.*, **366A**, 3969–3987, <https://doi.org/10.1098/rsta.2008.0137>.
- Leaith, W. R., and Coauthors, 2010: Cloud albedo increase from carbonaceous aerosol. *Atmos. Chem. Phys.*, **10**, 7669–7684, <https://doi.org/10.5194/acp-10-7669-2010>.
- Li, Z., and Coauthors, 2017: Influence of flue gas desulfurization (FGD) installations on emission characteristics of PM_{2.5} from coal-fired power plants equipped with selective catalytic reduction (SCR). *Environ. Pollut.*, **230**, 655–662, <https://doi.org/10.1016/j.envpol.2017.06.103>.
- Liu, S., and X. Z. Liang, 2010: Observed diurnal cycle climatology of planetary boundary layer height. *J. Climate*, **23**, 5790–5808, <https://doi.org/10.1175/2010JCLI3552.1>.
- Ma, N., and W. Birmili, 2015: Estimating the contribution of photochemical particle formation to ultrafine particle number averages in an urban atmosphere. *Sci. Total Environ.*, **512–513**, 154–166, <https://doi.org/10.1016/j.scitotenv.2015.01.009>.
- , and Coauthors, 2016: Variation of CCN activity during new particle formation events in the North China Plain. *Atmos. Chem. Phys.*, **16**, 8593–8607, <https://doi.org/10.5194/acp-16-8593-2016>.
- Mallet, M., and Coauthors, 2016: Overview of the Chemistry-Aerosol Mediterranean Experiment/Aerosol Direct Radiative Forcing on the Mediterranean Climate (ChArMEx/ADRMED) summer 2013 campaign. *Atmos. Chem. Phys.*, **16**, 455–504, <https://doi.org/10.5194/acp-16-455-2016>.
- Metzger, S., and Coauthors, 2012: Eddy-covariance flux measurements with a weight-shift microlight aircraft. *Atmos. Meas. Tech.*, **5**, 1699–1717, <https://doi.org/10.5194/amt-5-1699-2012>.
- , and Coauthors, 2013: Spatial resolution and regionalization of airborne flux measurements using environmental response functions. *Biogeosciences*, **10**, 2193–2217, <https://doi.org/10.5194/bg-10-2193-2013>.
- Mohnen, V. A., and J. P. Lodge, 1969: General review and survey of gas-to-particle conversions. *Proc. Seventh Int. Conf. on Condensation and Ice Nuclei*, Prague, Czech Republic, Prague Academia, 69–91.
- , and G. M. Hidy, 2010: Measurements of atmospheric nanoparticles (1875–1980). *Bull. Amer. Meteor. Soc.*, **91**, 1525–1539, <https://doi.org/10.1175/2010BAMS2929.1>.
- O’Dowd, C. D., and Coauthors, 2007: Airborne measurements of nucleation mode particles I: Coastal nucleation and growth rates. *Atmos. Chem. Phys.*, **7**, 1491–1501, <https://doi.org/10.5194/acp-7-1491-2007>.
- , and Coauthors, 2009: Airborne measurements of nucleation mode particles II: Boreal forest nucleation events. *Atmos. Chem. Phys.*, **9**, 937–944, <https://doi.org/10.5194/acp-9-937-2009>.
- Paasonen, P., K. Kupiainen, Z. Klimont, A. Visschedijk, H. A. C. Denier van der Gon, and M. Amann, 2016: Continental anthropogenic primary particle number emissions. *Atmos. Chem. Phys.*, **16**, 6823–6840, <https://doi.org/10.5194/acp-16-6823-2016>.
- Pan, D., and Coauthors, 2016: Emission and formation characteristics of aerosols from ammonia-based wet flue gas desulfurization. *Energy Fuels*, **30**, 666–673, <https://doi.org/10.1021/acs.energyfuels.5b01677>.
- Petäjä, T., and Coauthors, 2016: BA ECC: A field campaign to elucidate the impact of biogenic aerosols on clouds and climate. *Bull. Amer. Meteor. Soc.*, **97**, 1909–1928, <https://doi.org/10.1175/BAMS-D-14-00199.1>.
- Platis, A., B. Altstädter, B. Wehner, N. Wildmann, A. Lampert, M. Hermann, W. Birmili, and J. Bange, 2015: An observational case study on the influence of atmospheric boundary-layer dynamics on new particle formation. *Bound.-Layer Meteor.*, **158**, 67–92, <https://doi.org/10.1007/s10546-015-0084-y>.
- Pollak, L. W., and A. L. Metnieks, 1959: New calibration of photoelectric nucleus counters. *Geofis. Pura Appl.*, **43**, 285–301, <https://doi.org/10.1007/BF01993566>.

- Pueschel, R. F., and C. C. Van Valin, 1978: Cloud nucleus formation in a power plant plume. *Atmos. Environ.*, **12**, 307–312, [https://doi.org/10.1016/0004-6981\(78\)90212-3](https://doi.org/10.1016/0004-6981(78)90212-3).
- Riuttanen, L., and Coauthors, 2016: Observational evidence for aerosols increasing upper tropospheric humidity. *Atmos. Chem. Phys.*, **16**, 14 331–14 342, <https://doi.org/10.5194/acp-16-14331-2016>.
- Rönkkö, T., and Coauthors, 2017: Traffic is a major source of atmospheric nanocluster aerosol. *Proc. Natl. Acad. Sci. USA*, **114**, 7549–7554, <https://doi.org/10.1073/pnas.1700830114>.
- Rosenfeld, D., 2000: Suppression of rain and snow by urban and industrial air pollution. *Science*, **287**, 1793–1796, <https://doi.org/10.1126/science.287.5459.1793>.
- , and Coauthors, 2008: Flood or drought: How do aerosols affect precipitation? *Science*, **321**, 1309–1313, <https://doi.org/10.1126/science.1160606>.
- , M. Clavner, and R. Nirel, 2011: Pollution and dust aerosols modulating tropical cyclones intensities. *Atmos. Res.*, **102**, 66–76, <https://doi.org/10.1016/j.atmosres.2011.06.006>.
- Schobesberger, S., and Coauthors, 2013: Airborne measurements over the boreal forest of southern Finland during new particle formation events in 2009 and 2010. *Boreal Environ. Res.*, **18**, 145–163.
- Stull, R. B., 1988: *An Introduction to Boundary Layer Meteorology*. Kluwer, 670 pp.
- Suni, T., and Coauthors, 2008: Formation and characteristics of ions and charged aerosol particles in a native Australian Eucalypt forest. *Atmos. Chem. Phys.*, **8**, 129–139, <https://doi.org/10.5194/acp-8-129-2008>.
- Teller, A., and Z. Levin, 2006: The effects of aerosols on precipitation and dimensions of subtropical clouds: A sensitivity study using a numerical cloud model. *Atmos. Chem. Phys.*, **6**, 67–80, <https://doi.org/10.5194/acp-6-67-2006>.
- , L. Xue, and Z. Levin, 2012: The effects of mineral dust particles, aerosol regeneration and ice nucleation parameterizations on clouds and precipitation. *Atmos. Chem. Phys.*, **12**, 9303–9320, <https://doi.org/10.5194/acp-12-9303-2012>.
- Thiel, S., and Coauthors, 2008: Influence of clouds on the spectral actinic flux density in the lower troposphere (INSPECTRO): Overview of the field campaigns. *Atmos. Chem. Phys.*, **8**, 1789–1812, <https://doi.org/10.5194/acp-8-1789-2008>.
- Thornton, J. A., K. S. Virts, R. H. Holzworth, and T. P. Mitchell, 2017: Lightning enhancement over major oceanic shipping lanes. *Geophys. Res. Lett.*, **44**, 9102–9111, <https://doi.org/10.1002/2017GL074982>.
- Tröstl, J., and Coauthors, 2016: The role of low-volatility organic compounds in initial particle growth in the atmosphere. *Nature*, **533**, 527–531, <https://doi.org/10.1038/nature18271>.
- Twomey, S., 1974: Pollution and the planetary albedo. *Atmos. Environ.*, **8**, 1251–1256, [https://doi.org/10.1016/0004-6981\(74\)90004-3](https://doi.org/10.1016/0004-6981(74)90004-3).
- , 1977: On the minimum size of particle for nucleation in clouds. *J. Atmos. Sci.*, **34**, 1832–1835, [https://doi.org/10.1175/1520-0469\(1977\)034<1832:OTMSOP>2.0.CO;2](https://doi.org/10.1175/1520-0469(1977)034<1832:OTMSOP>2.0.CO;2).
- Väänänen, R., and Coauthors, 2016: Vertical and horizontal variation of aerosol number size distribution in the boreal environment. *Atmos. Chem. Phys. Discuss.*, <https://doi.org/10.5194/acp-2016-556>.
- Wehner, B., and Coauthors, 2010: Observations of turbulence-induced new particle formation in the residual layer. *Atmos. Chem. Phys.*, **10**, 4319–4330, <https://doi.org/10.5194/acp-10-4319-2010>.
- Went, F. W., 1964: The nature of Aitken nuclei in the atmosphere. *Proc. Natl. Acad. Sci. USA*, **51**, 1259–1267, <https://doi.org/10.1073/pnas.51.6.1259>.
- , 1966: On the nature of Aitken condensation nuclei. *Tellus*, **18**, 549–556, <https://doi.org/10.3402/tellusa.v18i2-3.9350>.
- Whitby, K. T., B. K. Cantrell, and D. B. Kittelson, 1978: Nuclei formation rates in a coal-fired power plant plume. *Atmos. Environ.*, **12**, 313–321, [https://doi.org/10.1016/0004-6981\(78\)90213-5](https://doi.org/10.1016/0004-6981(78)90213-5).
- Xausa, F., and Coauthors, 2018: Advancing global aerosol simulations with size-segregated anthropogenic particle number emissions. *Atmos. Chem. Phys.*, **18**, 10 039–10 054, <https://doi.org/10.5194/acp-18-10039-2018>.